The Contribution of Indian Ocean Sea Surface Temperature Anomalies on Australian Summer Rainfall during El Niño Events

ANDRÉA S. TASCHETTO AND ALEX SEN GUPTA

Climate Change Research Centre, University of New South Wales, Sydney, New South Wales, Australia

HARRY H. HENDON

Centre for Australian Weather and Climate Research, Bureau of Meteorology, Melbourne, Victoria, Australia

CAROLINE C. UMMENHOFER AND MATTHEW H. ENGLAND

Climate Change Research Centre, University of New South Wales, Sydney, New South Wales, Australia

(Manuscript received 8 June 2010, in final form 23 February 2011)

ABSTRACT

This study investigates the impact of Indian Ocean sea surface temperature (SST) anomalies on the atmospheric circulation of the Southern Hemisphere during El Niño events, with a focus on Australian climate. During El Niño episodes, the tropical Indian Ocean exhibits two types of SST response: a uniform ''basinwide warming'' and a dipole mode—the Indian Ocean dipole (IOD). While the impacts of the IOD on climate have been extensively studied, the effects of the basinwide warming, particularly in the Southern Hemisphere, have received less attention. The interannual basinwide warming response has important implications for Southern Hemisphere atmospheric circulation because 1) it accounts for a greater portion of the Indian Ocean monthly SST variance than the IOD pattern and 2) its maximum amplitude occurs during austral summer to early autumn, when large parts of Australia, South America, and Africa experience their monsoon. Using observations and numerical experiments with an atmospheric general circulation model forced with historical SST from 1949 to 2005 over different tropical domains, the authors show that the basinwide warming leads to a Gill–Matsuno-type response that reinforces the anomalies caused by changes in the Pacific as part of El Niño. In particular, the basinwide warming drives strong subsidence over Australia, prolonging the dry conditions during January–March, when El Niño–related SST starts to decay. In addition to the anomalous circulation in the tropics, the basinwide warming excites a pair of barotropic anomalies in the Indian Ocean extratropics that induces an anomalous anticyclone in the Great Australian Bight.

1. Introduction

Australian climate is affected by the surrounding oceans, particularly by variations in tropical Pacific and Indian Ocean sea surface temperature (SST). While El Niño–Southern Oscillation (ENSO) is the primary mode affecting Australian climate over the north and east throughout the year, variations of SST in the Indian Ocean, via the Indian Ocean dipole (IOD), play a primary role in modulating rainfall in the southern regions during austral winter and early spring (Risbey et al. 2009 and references therein). The effect of the IOD on Australian climate has already been reported by many previous studies (e.g., Ashok et al. 2003; Ummenhofer et al. 2009a,b). The IOD, which is prominent in austral winter and spring, is characterized by an anomalous east–west SST gradient along the equatorial Indian Ocean. It supports an associated anomalous surface pressure and rainfall distribution, which in turn induces remote changes in circulation that drive anomalous rainfall conditions over southern Australia.

Although the IOD is the leading mode of SST variability in the Indian Ocean during austral winter and spring, it only accounts for 12% of the explained variance for all months in detrended SST from 1958 to 1998 (Saji et al. 1999). In fact, the first pattern of monthly tropical Indian Ocean SST variability is a basinwide

Corresponding author address: Andréa S. Taschetto, Climate Change Research Centre, University of New South Wales, Sydney NSW 2052, Australia.
E-mail: a.taschetto@unsw.edu.au

DOI: 10.1175/2011JCLI3885.1

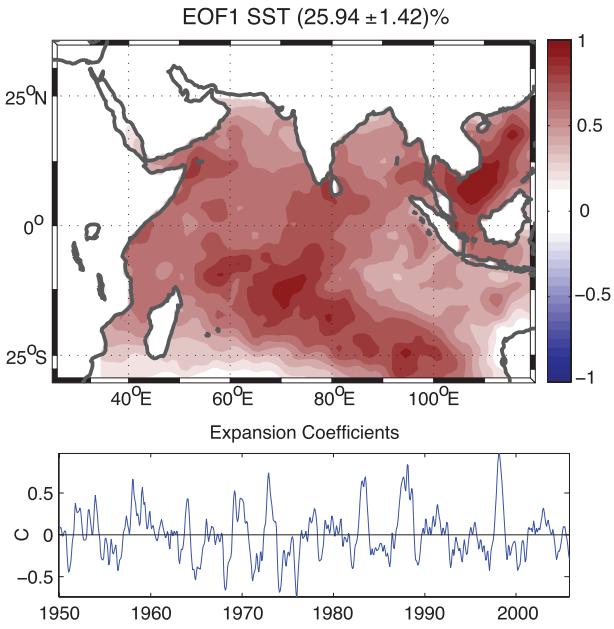

FIG. 1. (top) Leading EOF mode of monthly SST anomalies in the tropical IO, with (bottom) the time series of the associated expansion coefficients. Data based on the HadISST1 from December 1949 to November 2005. Eigenvalues indicate that this mode explains 25.94% of the total variance for monthly SST.

warming (e.g., Chambers et al. 1999), as shown here by an empirical orthogonal function (EOF) analysis (Fig. 1a). This pattern accounts for approximately 26% of the monthly tropical Indian Ocean SST variance from 1949 to 2005. An EOF analysis of the seasonal detrended SST (not shown) reveals a preference for the Indian Ocean basinwide warming to peak during austral summer and autumn. Despite appearing as the leading EOF, the basinwide warming is not referred to here as a mode of variability because it is essentially a forced response to ENSO processes in the Pacific and is not an independent oscillation (e.g., Klein et al. 1999; Lau and Nath 2000).

Typically, when El Niño develops in the middle of the year, the related anomalous Walker circulation generates an easterly wind stress anomaly over the equatorial Indian Ocean, so that the eastern (western) Indian Ocean becomes initially cold (warm) (e.g., Annamalai et al. 2003). The eastern cold anomaly, which normally occurs from July to November, rapidly disappears after the trade winds relax and switch to westerly in the eastern Indian Ocean during the onset of the Australian summer monsoon. Consequently, upwelling and surface cooling through the latent heat flux are reduced. Simultaneously, the atmospheric subsidence induced during the peak of El Niño events (i.e., November–December) reduces convection and cloud cover over the eastern Indian Ocean, thus increasing the net heat flux into the ocean (Klein et al. 1999). The anomalous Walker circulation also acts to decrease wind speed at the beginning of the austral summer. The reduction of wind speed, in conjunction with the weakening of the seasonal upwelling and the anomalous heat flux into the ocean, favors a rapid warming of the eastern Indian Ocean after December (e.g., Tokinaga and Tanimoto 2004). The anticyclonic wind anomalies also initiate downwelling Rossby waves (e.g., Masumoto and Meyers 1998; Chambers et al. 1999) that propagate westward, deepening the thermocline and sustaining the warming in the western Indian Ocean (Xie et al. 2002). The uniform basinwide warming thus reaches its maximum amplitude during late austral summer and autumn, approximately 3–4 months after the El Niño mature phase (Lau and Nath 2003).

The fact that the Indian Ocean basinwide warming is a response to El Niño events masks its importance in modulating atmospheric circulation. However, previous studies demonstrated its significance for the South and East Asian monsoons, the western Pacific region, Philippine Sea, South China Sea, and other Indian Ocean rim nations (e.g., Watanabe and Jin 2002; Annamalai et al. 2005; Yang et al. 2007; Li et al. 2008; Xie et al. 2009; Schott et al. 2009). Yang et al. (2009) show that the basinwide warming can also generate significant remote circumglobal teleconnections in the Northern Hemisphere midlatitudes during boreal summer.

Xie et al. (2009) hypothesized that the ENSO-induced Indian Ocean warming acts as a capacitor for the Indo-western Pacific climate. The peak of El Niño events during late austral spring–early summer leads to a warming of the tropical Indian Ocean (''charging'' the capacitor). The basinwide warming is maintained via ocean–atmosphere interactions within the tropical Indian Ocean, as described by Du et al. (2009), and persists through austral winter after the eastern Pacific SST anomalies have dissipated. The persistent Indian Ocean basinwide warming then acts as a discharging capacitor, exerting a delayed influence on the northwestern Pacific climate via a Gill–Matsuno response. Recently, Huang et al. (2010) showed that the tropical Indian Ocean–northwestern Pacific climate relationship has strengthened since the mid-1970s because of the intensification and persistence of the El Niño–induced Indian Ocean SST anomalies during the boreal summer.

Unlike the IOD, little is known about the direct climate impacts of the basinwide warming on the Southern Hemisphere circulation. In this study, we focus on austral summer and autumn, when the IOD variability is less prominent and the Indian Ocean basinwide warming has its greatest influence on the Southern Hemisphere climate. We show that during El Niño events, the January–March (JFM) Australian rainfall is modulated by the Indian Ocean as well as by tropical Pacific SST anomalies. In

addition, we assess the relative influence of the basinwide warming on the Southern Hemisphere circulation using an atmosphere general circulation model (AGCM).

2. Datasets and numerical experiments

The observational datasets used here consist of the global SST and sea ice data from the Hadley Centre [Met Office Hadley Centre Sea Ice and Sea Surface Temperature version 1 (HadISST1); Rayner et al. 2003] and gridded rainfall analyses from the Australian Bureau of Meteorology (BOM; Jones et al. 2009). The period analyzed in this study ranges from December 1949 to November 2005. The anomalies relative to the seasonal cycle were calculated by removing long-term monthly climatology over the entire period. In addition, the time series were linearly detrended to highlight the relationship between the Indian Ocean basinwide warming and Southern Hemisphere climate on interannual time scales. Previous studies have examined the impacts of the long-term Indian Ocean warming trend on regional climate (e.g., Luffman et al. 2010) and will not be addressed here.

The National Center for Atmospheric Research (NCAR) Community Atmospheric Model, version 3 (CAM3) was used to perform four experiments. A complete description of the CAM3 can be found in Collins et al. (2004). Each experiment consists of a seven-member ensemble, each forced with historical SST from December 1949 to November 2005 over different domains and with a repeating mean seasonal SST climatology elsewhere. The different domains were 1) the tropical Indian Ocean (IO); 2) the tropical Pacific Ocean (PO); and 3) the tropical Indian and Pacific Oceans (IO+PO), where the tropics are defined from 30°S to 30°N, and the Indian and Pacific Oceans are longitudinally bounded at 130°E and by the African and American continents. To reduce spurious atmospheric responses at the domain boundaries, the historical SST fields were linearly damped out over a distance of approximately 1000 km. A fourth experiment was performed with monthly varying SST over the global oceans (GO) to assess the realism of the model compared to observations. In addition, a control experiment was performed that had climatological SST forcing globally (CTRL).

To account for unforced internal variability, each ensemble member was started from slightly different initial conditions. The ensemble mean of each experiment was analyzed here for precipitation, geopotential height, vertical velocity, sea level pressure, asymmetric streamfunction, and wind fields.

Previous studies have reported biases in the accurate simulation of the Asian–Australian monsoon system using uncoupled AGCM experiments due to the lack of monsoon–ocean interactions (Wang et al. 2008 and references therein). This poor representation in the monsoon regions seems to be aggravated for the Northern Hemisphere compared to the Southern Hemisphere. For instance, Wang et al. (2004) concluded that most of the models participating in the Atmospheric Model Intercomparison Project (AMIP) reproduced quite realistic low-level circulation anomalies and the variability of the Australian monsoon region, but they failed to simulate a realistic Indian monsoon. Similarly, Zhou et al. (2009) examined the Asian–Australian monsoon variability simulated by AGCMs forced by prescribed historical SSTs and concluded that, despite limitations in the Asian monsoon representation, the (austral summer) Australian monsoon is quite well simulated because the December–February (DJF) season has the highest skill in the AMIP-style runs.

Figure 2 shows the observed/reanalyzed versus simulated climatology of rainfall and sea level pressure using the GO experiment. Generally, the sea level pressure climatology is slightly overestimated in the model compared to the reanalysis. In addition, some local features of the rainfall climatology are not well represented in the model, such as the east–west precipitation pattern in Tasmania and the increased rainfall along the eastern coast. Nevertheless, the large-scale pattern is well captured by the model, given the absence of ocean–atmosphere interaction and the coarse resolution of the model. For instance, the CAM3 represents well the pressure trough and high rainfall intensities when the monsoon is active (i.e., during austral summer), and the high-pressure center and low rainfall values over the southern half of Australia during austral winter.

The annual cycle of rainfall averaged over northern Australia is slightly overestimated in the simulation compared to observations; however, the model reproduces the seasonality very well. Previous studies have reported the limitations of the CAM3 in simulating extreme events and trends in rainfall and temperature over Australia (Alexander and Arblaster 2009); however, this is not addressed in this study. For our purposes, both Australian rainfall and the circulation climatologies are satisfactorily well represented by the NCAR CAM3 model.

3. Results

a. Impacts on Australian rainfall

Figure 1 shows the spatial signature of the leading basinwide warming. Because of the inhomogeneity in the SST observations across the Indian Ocean SST prior to

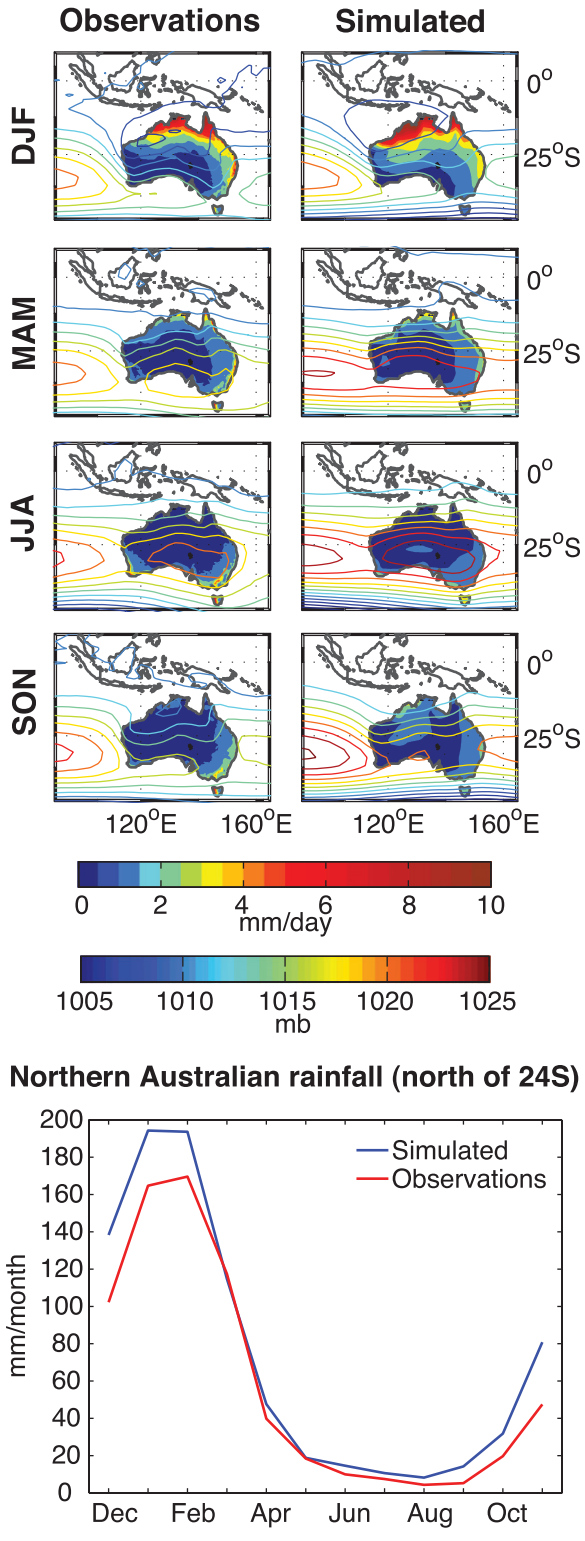

FIG. 2. (top) Seasonal climatologies of rainfall (color shaded over Australia) and sea level pressure (contoured) for (left) observations (BOM data) and reanalysis [National Center for Atmospheric Research (NCEP)–NCAR] and (right) the simulated fields from the GO experiment. (bottom) Annual cycle of rainfall averaged over northern Australia (north of 24°S).

the satellite era (Deser et al. 2010, their Fig. 3), the EOF analysis has also been performed for the period December 1981–November 2005. In addition, the analysis was carried out with the National Oceanic and Atmospheric Administration (NOAA) Optimum Interpolation Sea Surface Temperature, version 2 (OISSTv2) data (Reynolds et al. 2002) to account for any biases in the interpolation method of the gridded datasets. The first principal components between the entire period and the postsatellite era and between HadISST1 and NOAA OISSTv2 data are essentially the same (not shown). The correlation coefficient of the principal component time series between these datasets is 0.925 for the same period.

Figure 3 shows the month-by-month standard deviation of the IOD, Indian Ocean basinwide warming (IOBW), and Niño-3.4 as well as the annual cycle of correlations between them. The principal component time series shown in Fig. 1 is used here as the index for the IOBW, while the IOD index is calculated according to Saji et al. (1999).

Although the IOBW appears as the leading pattern of variability in the Indian Ocean, it acts primarily during the first half of the year, as shown by the annual cycle of the standard deviation of the IOBW index (Fig. 3b, blue line). In contrast, the second half of the year is dominated by the IOD mode (Fig. 3a, blue line), particularly during August–October.

Both the IOBW and IOD reveal significant correlations with ENSO during those months when the indices have a large standard deviation. The significant correlation coefficient of approximately 0.6 during September–November (SON) between Niño-3.4 and the IOD indices (Fig. 3a, red line) does not necessarily imply a dynamical link between these two phenomena. It is a statistical reflection of the co-occurrence of approximately 45% IOD events with ENSO (Meyers et al. 2007). Although some positive (negative) IOD events occur during the same year as El Niño (La Niña), previous studies support the hypothesis that the IOD is also a distinct coupled ocean–atmosphere phenomenon (e.g., Saji and Yamagata 2003). Li et al. (2003) also argue that the IOD is independent of ENSO, but the latter is one of the major triggering mechanisms of the former. A review of the IOD–ENSO relationship can be found in Schott et al. (2009).

The strong ($r > 0.7$) Niño-3.4 and IOBW correlation (Fig. 3b, solid red line) during JFM results from the dynamical link between these two phenomena. As El Niño anomalies decay, the correlation between the IOBW and Niño-3.4 indices weakens; however, it remains significant up to June. The maximum standard deviation of the IOBW occurs 2 months after the maximum Niño-3.4 (Figs. 3b and 3c, blue lines), at a time

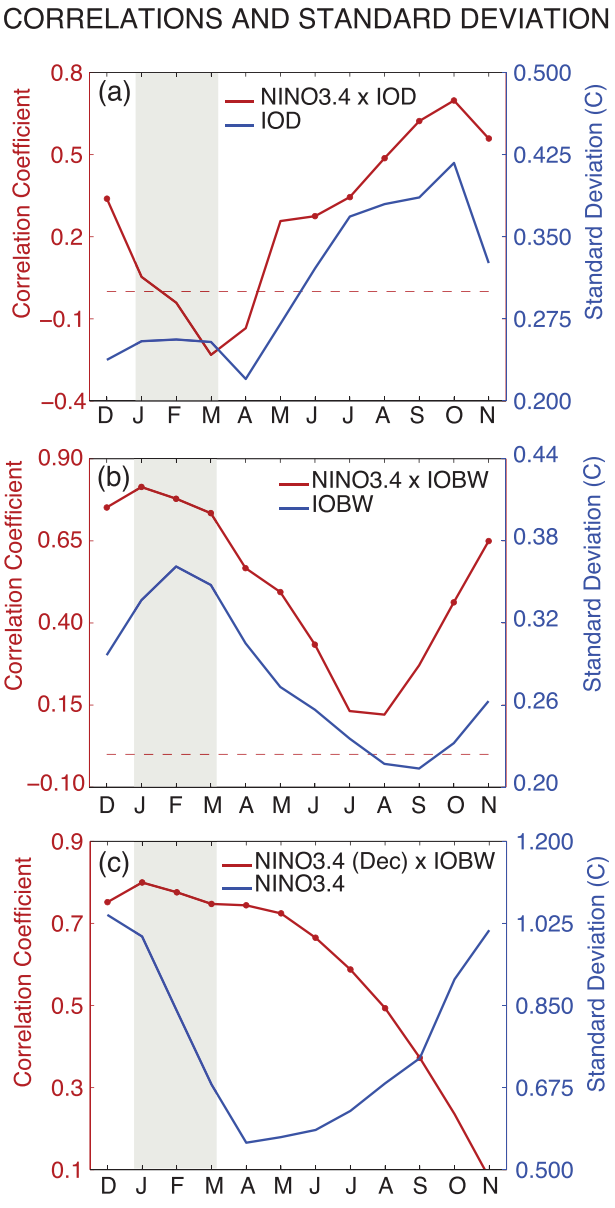

FIG. 3. Annual cycle of the standard deviation of the (a) IOD, (b) IOBW, and (c) Niño-3.4 indices (blue) and month-by-month correlations between the Niño-3.4 index and the (a) IOD and (b) IOBW and (c) lagged correlation between the IOBW index and the Niño-3.4 index fixed at the peak of El Niño (December) (red). Circles show correlation coefficients significant at the 95% confidence level based on a Student's *t* test. Gray band shows the months when the IOBW index peaks.

when El Niño SST anomalies are rapidly decaying in the tropical Pacific (Fig. 3c, blue line). Figure 3c (solid red line) shows the correlations between the December Niño-3.4 index (i.e., the peak Niño-3.4 standard deviation, blue line) and the monthly varying IOBW index. The ENSO-induced Indian Ocean warming extends throughout austral autumn and winter. The persistence

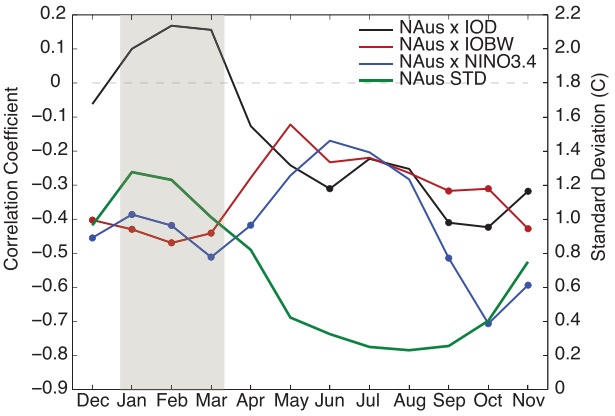

FIG. 4. Annual cycle of 3-month running-mean correlation between northern Australian rainfall (north of 24°S) and Niño-3.4 (blue), IOBW (red), and IOD (black) indices. Circles show correlation coefficients significant at the 95% confidence level based on a Student's *t* test. The gray band shows the months when the IOBW index peaks. The green line represents the standard deviation of northern Australia rainfall.

of the SST warming in the tropical Indian Ocean until austral winter after the peak of El Niño is consistent with the capacitor effect of the tropical Indian Ocean proposed by Xie et al. (2009).

The importance of the IOBW for Australian climate lies in the fact that its maximum intensity occurs during JFM, when the monsoon is active. The Australian monsoon generally starts in December and ends in March (Suppiah 1992), bringing more than 70% of the total annual rainfall during this time of the year for the tropical regions. To demonstrate that the Australian tropical climate is affected by the Indian Ocean SST anomalies, Fig. 4 shows the month-by-month correlation between the IOBW index and rainfall averaged north of 24°S over Australian land areas. To smooth the high variability of the monthly rainfall time series, the correlation in January takes into account the DJF mean for both the IOBW index and precipitation; the correlations in February are calculated using the JFM mean time series; and so on. For comparison, the annual cycles of the correlation between precipitation and the IOD and Niño-3.4 indices are also presented in Fig. 4.

The strongest negative correlations between Australian rainfall and the IOBW index are observed during JFM, coinciding with the peak of the basinwide warming. Similarly, the IOD is significantly correlated with Australian rainfall during SON, when the phenomenon peaks. However, the impact of the IOBW is greater than that of the IOD on northern Australian rainfall, simply because most of the rainfall occurs in JFM, when the monsoon is active. This is demonstrated by the monthly standard deviation depicted by the green line in Fig. 4,

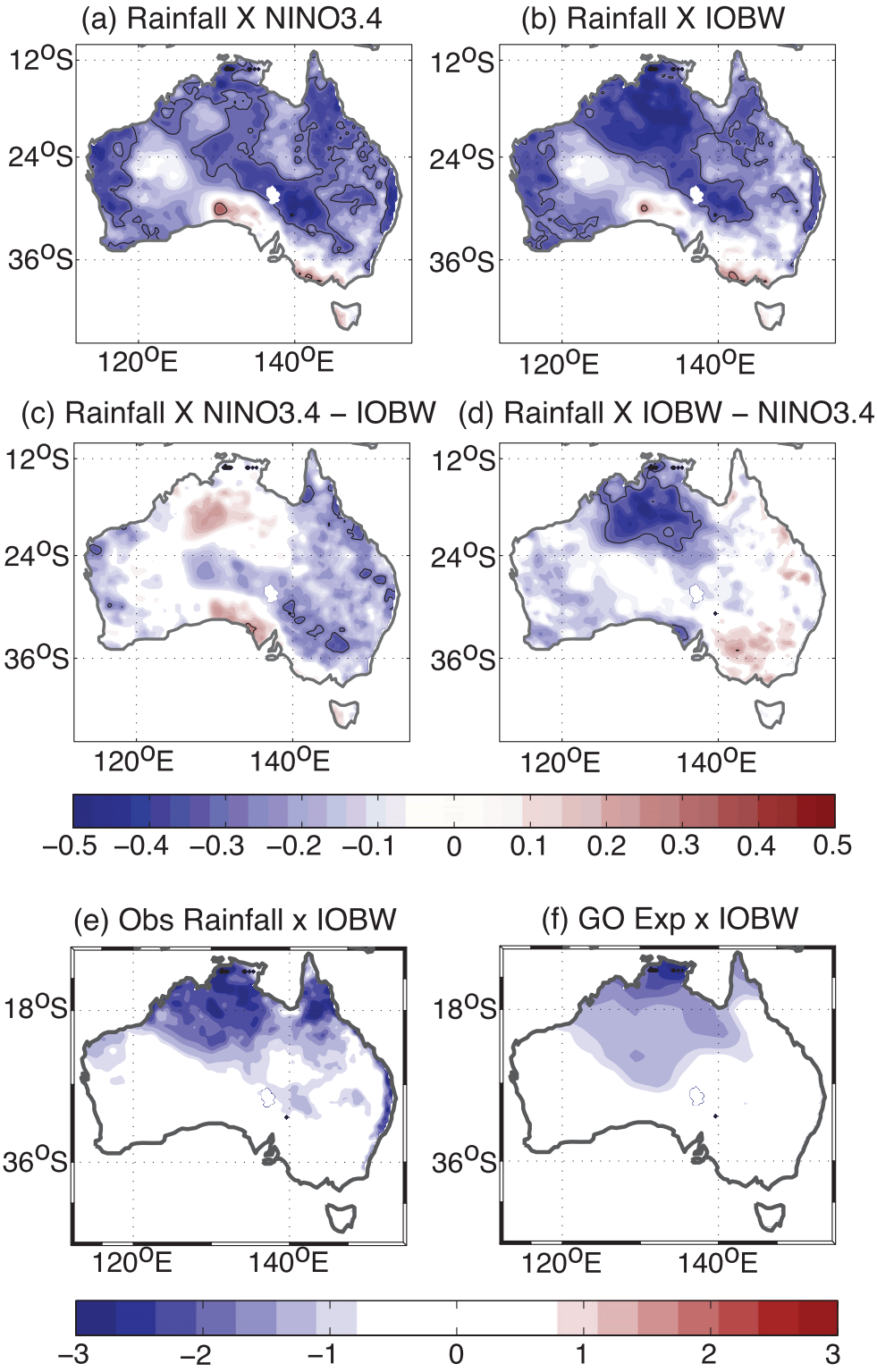

FIG. 5. Spatial structure of the temporal correlation between JFM Australian rainfall from BOM and the JFM (a) Niño-3.4 and (b) IOBW indices. Partial correlations between JFM Australian rainfall and (c) the JFM Niño-3.4 index without the IOBW index and (d) the IOBW without the Niño-3.4 index. Areas within the thin black line are statistically significant at the 95% confidence level based on a Student's *t* test. Regressions between the IOBW index and (e) the observed JFM rainfall from BOM and (f) the simulated rainfall in the GO experiment.

with maximum values from December to March and minimum values from June to October.

Figure 4 also shows that correlations with the Niño-3.4 index and Australian rainfall are significant during the same months as for the IOBW and IOD, again indicating that both phenomena have a statistical connection to tropical Pacific variability. Untangling the relative contributions of Indian and Pacific Ocean SST variability on JFM rainfall, given that the IOBW is a forced response to ENSO, is therefore a difficult task.

To address the problem of multiple drivers, a partial correlation is commonly used. Here, the influence of one driver is removed prior to a correlation with the other driver. JFM rainfall is significantly correlated with El Niño (Fig. 5a); however, any statistically significant response essentially disappears when the IOBW index is removed from the time series before calculating the correlations (Fig. 5c). In comparison, when a partial correlation is performed between the IOBW index and Australian rainfall with the effect of the Niño-3.4 removed (Fig. 5d), although the correlations are much reduced, they remain significant over much of the northwestern region (Fig. 5d). This suggests that despite being a response to ENSO, the basinwide warming may be the primary driver of anomalous atmospheric circulation that favors below-average rainfall over northwestern Australia. These results should be viewed with caution, however. In particular, this technique assumes a linear relationship between El Niño, the IOBW, and Australian rainfall. In addition, the basinwide warming and Niño-3.4 are highly correlated (Fig. 3b), and the amplitude of the IOBW index is considerably reduced when removing the effect of Niño-3.4, making interpretation difficult.

To address these uncertainties, we make use of numerical experiments. A preliminary assessment of the modeled rainfall response to the Indian Ocean warming in the GO experiment shows good agreement with observations, as revealed by the regression of the IOBW index on to Australian rainfall (Figs. 5e and 5f).

b. Tropical teleconnections

A more robust way of separating the relative effects of the Pacific and Indian Ocean variability can be done using atmospheric model experiments with prescribed SST forcing. Here, we examine the relative impact of the tropical Pacific and Indian Oceans in experiments IO, PO, and IO+PO. Figure 6 shows the simulated JFM vertical velocity anomaly averaged between 10°S and 10°N regressed on to the observed IOBW index. Similarly, Figs. 6 and 7 show the simulated JFM large-scale circulation at low and high levels of the atmosphere represented by sea level pressure, horizontal winds, and asymmetric streamfunction anomalies regressed onto the IOBW index.

In the IO experiment (where interannual variability is only present in the tropical Indian Ocean), the basinwide warming is associated with an overall decrease in sea level pressure and an anomalous expansion of the high troposphere over the Indian Ocean as a response to the underlying SST warming (Figs. 6a and 7a). The anomalous sea level pressure over the ocean warming generates a pressure gradient that induces anomalous trade winds over Indonesia and westerly wind anomalies over Africa. As a consequence, a zone of low-level convergent flow takes place over the central-western equatorial Indian Ocean. By continuity, local ascending motion occurs over the heating source, as shown by the vertical velocity anomalies over the Indian Ocean longitudes from 30° to 110°E (Fig. 6a). This provides a Walker-type circulation with updraft over the convergence area and subsequent sinking motion eastward to the heating source. Off the coast of Madagascar, a cyclonic circulation anomaly occurs while an anomalous anticyclone is located over the northwestern coast of Australia (Fig. 7a).

The anomaly patterns shown in Figs. 7 and 8 resemble the Gill–Matsuno response (e.g., Gill 1980) to diabatic heating across the equator, with the propagation of equatorially trapped Kelvin waves to the east and, by conservation of vorticity, a return flow to the western margins of the heating source. This response is also clearly represented in Fig. 8a by the quadrupole anomaly pattern in the simulated asymmetric streamfunction in the high troposphere. The baroclinic Gill–Matsuno response to the heating in the tropical Indian Ocean is associated with a pair of upper-atmosphere anticyclonic anomalies that straddle the equator at about 60°E and overlie cyclonic anomalies in the lower troposphere (Figs. 6a and 7a). In addition, an anomalous cyclone associated with upper-level convergence is located over Australia (Fig. 8a). This generates a subsequent subsidence across Australia, thus inhibiting convection and causing dry conditions in this region. This response suggests that the IOBW can independently reduce rainfall over Australia via changes in the Walker circulation. This is consistent with the results of Lau and Nath (2000), who obtained drier conditions over northern Australia during DJF in an experiment with global-varying prescribed SST compared to a simulation forced with SST anomalies varying only over the tropical Pacific.

The PO experiment (Fig. 6b) shows a strong upward motion in the central Pacific associated with the El Niño SST anomalies. However, the associated downward motion between the longitudes 120° and 160°E is weaker than in the IO case. The JFM response from realistic

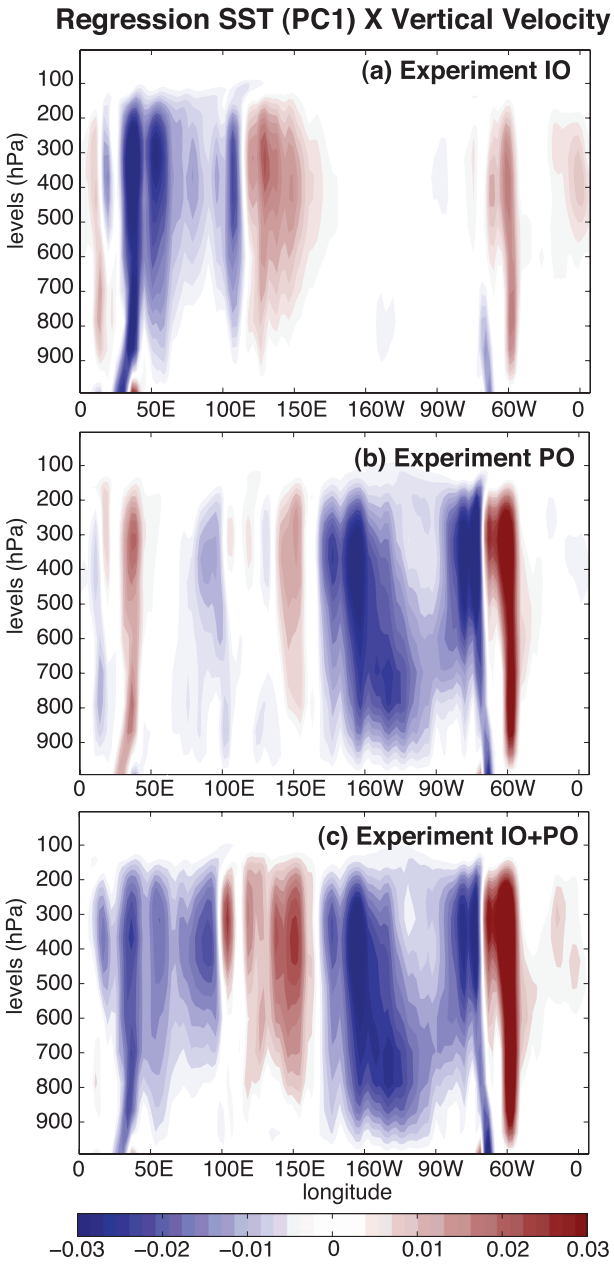

FIG. 6. Simulated JFM vertical velocity anomalies (Pa s^{-1}) averaged between 10°S and 10°N regressed onto the leading principal component of the observed IOBW index: (a) IO, (b) PO, and (c) IO+PO experiments. Blue (red) regions indicate an upward (downward) motion.

SST forcing over the Pacific and Indian Oceans (i.e., from the IO+PO experiment) reveals a strong subsidence extending across all Australian longitudes (Fig. 6c), resulting from the rising motion over both tropical oceans. The response obtained in the IO+PO experiment seems to be a linear combination of the individual IO and PO experiments. The Gill–Matsuno-related pair of anticyclones straddling the equator is a clear response, in the PO experiment, to El Niño (Fig. 8b). No significant circulation anomaly occurs over Australia at 200 hPa (Fig. 8b), although an anticyclone at low levels is seen over the northwestern coast of the continent (Fig. 7b). In addition to the tropical teleconnections driven by the warm SST in the tropical Indian Ocean, there is also an atmospheric response that extends into the higher southern latitudes.

c. *Extratropical teleconnections*

Figure 9 shows the simulated JFM large-scale circulation in the Southern Hemisphere extratropics represented by the geopotential height anomalies and horizontal winds at 200 hPa regressed onto the IOBW index.

In the IO experiment (Fig. 9a), a wave train pattern of equivalent barotropic anomalies emanates from the tropical Indian Ocean to higher southern latitudes, presumably resulting from the tropical diabatic heating anomalies (e.g., Hoskins and Karoly 1981) associated with the IOBW. Drumond and Ambrizzi (2008) showed that a warming in the subtropical Indian Ocean can produce a stationary Rossby wave train teleconnection to South America during DJF. Our result suggests a more confined response over the Indian Ocean sector during JFM, although preliminary analyses have shown that the Indian Ocean–South American teleconnection strengthens from austral autumn to winter (not shown). The wave pattern obtained here results in a strong equivalent barotropic anticyclonic anomaly in the Great Australian Bight, with associated easterly wind anomalies across extreme southern parts of the country.

Southern Australian rainfall is dependent on the location and intensity of extratropical systems in the storm tracks. The anomalous circulation simulated in the Australian extratropics in the IO experiment suggests a possible influence of the IOBW in modulating rainfall over southern Australia. The anticyclone anomaly would lead to below-normal rainfall conditions by weakening the westerlies and reducing the number of extratropical lows and frontal systems reaching the southern regions of the country. The impacts of any Indian Ocean SST variability on the southern parts of Australia would, however, be larger during austral winter and spring, when the region experiences its rainy season. For instance, Ashok et al. (2003) found significant negative correlations between June and September rainfall over southern Australia and IOD events. Saji et al. (2005) found that southern Australia, subtropical South America, and South Africa experience warmer air temperatures with positive IOD events during SON, driven by a wave train emanating from the eastern Indian Ocean and

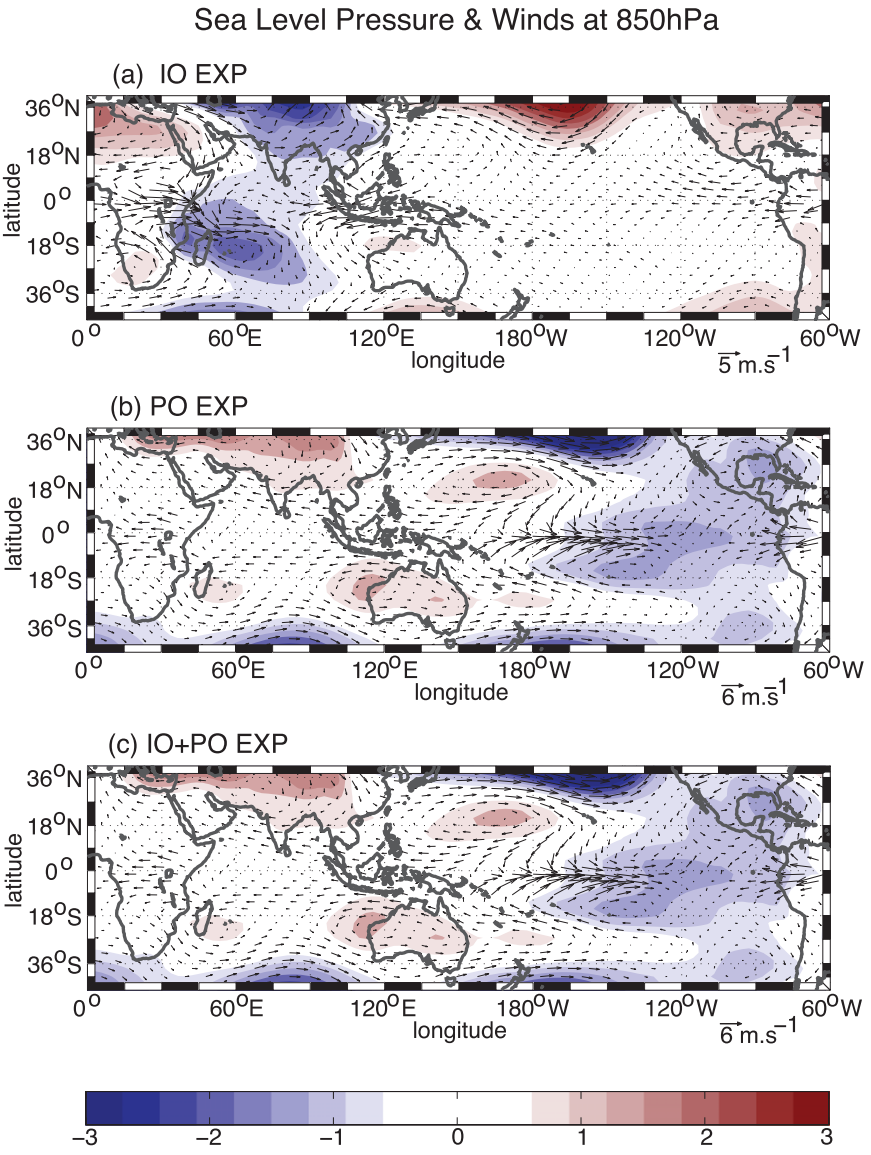

FIG. 7. Simulated JFM anomalies of sea level pressure (mb) and winds (m s^{-1}) at 850 hPa regressed onto the IOBW index: (a) IO, (b) PO, and (c) IO+PO experiments. Colored areas represent a response significant at the 95% confidence level according to a two-sided *t* test.

propagating along the subtropical and subpolar jet streams. Chan et al. (2008) also reported a similar wave train teleconnection associated with IOD events during SON that modulates rainfall variability in South America. Here, we show that, during austral summer, the IOBW generates a wavelike pattern more confined in the Indian Ocean sector.

The wave train/height anomalies over the extratropics present a different pattern when the model is forced by the Pacific SST anomalies only, with the signal south of Australia largely absent (Fig. 9b). Instead, the atmospheric response appears across all the circumpolar latitudes of the Southern Hemisphere. The combined Indian and Pacific SST forcings simulate a much stronger extratropical response in the IO+PO experiment (Fig. 9c). In particular, the anticyclonic anomaly to the south of Australia in the Bight is damped in the combined experiment, producing a more annular pattern with a wavenumber 3–like response in the extratropics during JFM. This is consistent with the findings of Carvalho et al. (2005) and L'Heureux and Thompson (2006), who showed that the Southern Hemisphere circulation response to ENSO during austral summer includes a component that projects onto the southern annular mode.

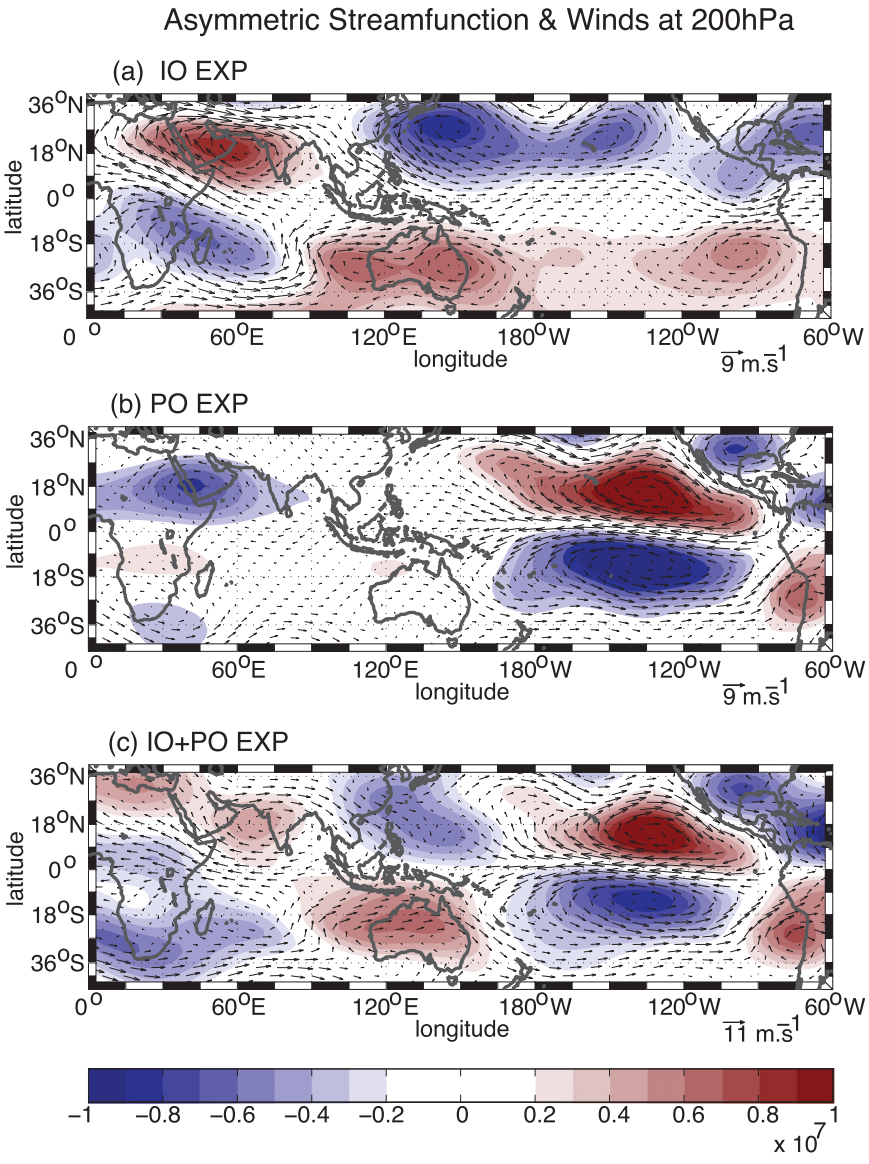

FIG. 8. Simulated JFM anomalies of asymmetric streamfunction (m^2 s^{-1}) and winds (m s^{-1}) at 200 hPa regressed onto the IOBW index: (a) IO, (b) PO, (c) IO+PO experiments. Colored areas represent a response significant at the 95% confidence level according to a two-sided *t* test.

4. Conclusions

In this study, we examined the influence of the Indian Ocean basinwide warming on Southern Hemisphere circulation using observations and a set of AGCM experiments for the period December 1949 to November 2005. The analyses shown here were also confirmed for the postsatellite era, from December 1981 to November 2005, and with different SST datasets (i.e., HadISST and NOAA).

Previous studies on the impacts of the Indian Ocean on Australian climate have tended to focus on the IOD phenomenon. The climate effects of the basinwide warming have been largely overlooked, in part because the IOBW is a response to El Niño events. However, given that the IOBW is the leading EOF pattern of Indian Ocean SST variability and its signal persists a few months after the El Niño decay, its impact cannot be neglected. Moreover, the IOBW generally peaks when the monsoon season is active in the Southern Hemisphere. Here, we have shown that Australian rainfall is affected not only by the direct SST warming in the tropical Pacific during El Niño events but also by the indirect effect of ENSO on the Indian Ocean via the

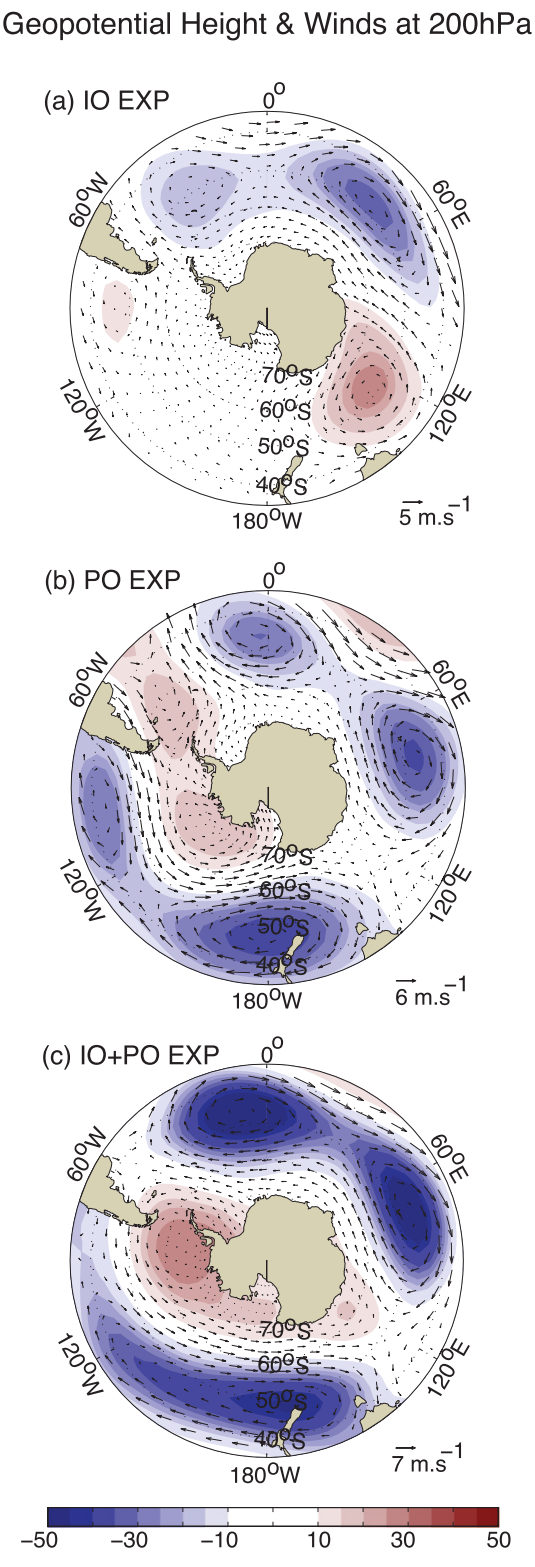

FIG. 9. As in Fig. 8, but of geopotential height (m) and winds (m s^{-1}).

IOBW. Separating the relative influence of the IOBW from ENSO is difficult, as they are strongly correlated. However, given that future changes may affect variability in the basins differently, it is important to understand their individual roles. An attempt is made here using partial correlation analysis in observations and AGCM simulations.

The mechanisms that influence the climate response to the basinwide warming of the Indian Ocean can be divided into two categories: 1) tropical teleconnections via the Gill–Matsuno response and 2) extratropical links via a wave train pattern.

The IOBW leads to an adjustment of the Walker cell over the Indian Ocean that enhances the circulation anomalies caused by El Niño events in the Pacific. The Indian Ocean warming induces a region of anomalous low pressure that leads to anomalous wind convergence and, by continuity, upward motion throughout the troposphere occurs over the warm waters in the tropical Indian Ocean basin. This increases the vertical moisture advection from low to mid- and high levels of the atmosphere, favoring enhanced diabatic heating that in turn drives a Gill–Matsuno-type response over the tropical Indian Ocean. The Gill–Matsuno response generates a baroclinic circulation anomaly, characterized by an anomalous anticyclone at 200 hPa, associated with convergence at upper levels over Australia. Consequently, enhanced subsidence inhibits convection and the formation of clouds, directly generating dry conditions across the continent.

Based on the numerical experiments, the subsidence is considerably weaker in the PO experiment compared to the IO experiment. The simulations therefore suggest that Indian Ocean anomalies might in fact be the primary cause of the dry conditions over Australia—although these anomalies are ultimately caused by Pacific SST variability. The subsidence in the IO+PO experiment seems to be a linear combination of the Pacific and Indian Ocean forcings.

The results found in this study are consistent with the Indian Ocean capacitor effect proposed by Xie et al. (2009). Here, we show that the ''capacitor effect'' takes the form of the IOBW for the Southern Hemisphere. The persistence of the IOBW through austral autumn exerts a delayed response on northwestern Australia circulation and rainfall, prolonging the dry conditions initiated by El Niño events. Given that the IOBW can persist throughout austral autumn and winter (as in Xie et al. 2009 and in our Fig. 2c), the indirect effect of El Niño on Australian rainfall via the Indian Ocean warming can extend through and beyond the monsoon season.

In addition to the Gill–Matsuno response, an equivalent barotropic wave pattern is excited in the Southern

Hemisphere extratropics by the diabatic heating anomalies associated with the tropical rainfall variation induced by the SST warming. In the IO experiment, the signal is more confined to the Indian Ocean sector. An anticyclone is located over the Great Australia Bight, suggesting a weakening of the westerlies and a reduction in the synoptic systems affecting rainfall in the southern regions of the continent. The experiment forced with the Pacific SST only and the combined response in the IO+PO experiment produces a more annular anomaly.

The significant extratropical teleconnection over the Indian Ocean sector in the IO experiment suggests that the IOBW has the potential to modulate the ENSO Rossby wave train teleconnection over the southern mid- to high latitudes. It is likely that the background circulation of the atmosphere plays a role in influencing this remote response via the mean state of the subtropical jets, which can act as waveguides to tropically forced atmospheric anomalies (Ambrizzi and Hoskins 1997). For instance, Lee et al. (2009) demonstrate that the circumpolar wave train pattern in the summer hemisphere is generally weaker than in winter because the subtropical jet is farther from the heating latitude. Because the warming from the basinwide warming can extend farther toward this jet in the Indian Ocean than ENSO variability in the Pacific Ocean, the weaker summer subtropical jet is still able to host a robust stationary wave train in the IO experiment.

It is important to mention that the AGCM experiments do not take into account any feedback associated with the ocean, but instead they provide a direct tool to assess the impact of the SST on the atmospheric circulation. The use of AGCM simulations provides a more controlled experimental design for our purposes without adding complexity. Another decisive factor for using an AGCM here—and not coupled climate models—lies in the teleconnection bias reported by Cai et al. (2009). The authors documented the poor ability of the Coupled Model Intercomparison Project phase 3 (CMIP3) models in simulating a correct rainfall–ENSO teleconnection over the Maritime Continent. They show that most of the CMIP3 models have a cold tongue bias in the equatorial Pacific and a warm pool located too far west. Consequently, Australia suffers an unrealistic ENSO–rainfall teleconnection, with more models showing a significant correlation over western rather than eastern Australia.

An alternative technique would be to use a coupling experimental design. Using a suite of experiments forced with prescribed SST in the tropical Pacific and a mixed layer ocean elsewhere, Lau and Nath (2000, 2003) found that the IOBW tends to offset the negative Australian rainfall anomaly caused by ENSO during the second half of the year. Although our results suggest that the IOBW reinforces the El Niño impacts during JFM, we also found that the subsiding anomaly over the Australian longitudes (Fig. 6a) tends to weaken during JJA (not shown), which a priori agrees with Lau and Nath's (2000) findings; however, it could also be due to the weakening of the IOBW itself and the strengthening of the IOD during this time of the year.

A complicating factor in the IOBW–ENSO relationship arises from modified responses due to different types of El Niño. Here, we used the Niño-3.4 index, which shows the strongest links with Australian climate. However, the Niño-3.4 region experiences warming during both canonical and El Niño Modoki events (Ashok et al. 2007), and thus the Niño-3.4 index does not distinguish among these flavors. Wang and Hendon (2007) observed distinct impacts on Australian rainfall to different flavors of El Niños. Taschetto and England (2009) and Taschetto et al. (2009) showed that El Niño Modoki episodes tend to be associated with below-normal rainfall over northern Australia during December and March–May, driven by anomalous subsidence from a shifted Walker circulation. They also show that, during January and February, northwestern Australia tends to experience above-normal rainfall during Modoki events because of the interaction of the anomalous SST warming around the date line and the climatologically enhanced diabatic heating generated by the setup of the South Pacific convergence zone (Taschetto et al. 2010). The sharp transition in the rainfall conditions from February to March over northern Australia during Modoki events may possibly be intensified by the IOBW. However, whether El Niño Modoki events can induce a basinwide warming in the Indian Ocean is still unresolved.

Finally, although observations support the findings of this study, it should be noted that the results obtained with the numerical experiments may be model dependent. Future studies, possibly using the new generation of climate models currently coming online, are needed to test the robustness of our results.

This study shows the importance of the Indian Ocean basinwide warming in modulating and prolonging the JFM rainfall and circulation anomalies over Australia associated with El Niño events, historically almost entirely attributed to tropical Pacific SST variability. In addition, this study demonstrates the potential of the Indian Ocean to not only affect regional climate but also drive global extratropical teleconnections.

Acknowledgments. The HadISST was provided by the Met Office Hadley Centre. The Australian Bureau of Meteorology provided the precipitation data. Use of NCAR's CCSM3 model is gratefully acknowledged. The

model simulations were run at the Australian Partnership for Advanced Computing National Facility. This research was supported by the Australian Research Council.

REFERENCES

Alexander, L. V., and J. Arblaster, 2009: Assessing trends in observed and modelled climate extremes over Australia in relation to future projections. *Int. J. Climatol.,* **29,** 417–435.

Ambrizzi, T., and B. J. Hoskins, 1997: Stationary Rossby-wave propagation in a baroclinic atmosphere. *Quart. J. Roy. Meteor. Soc.,* **123,** 919–928.

Annamalai, H., R. Murtugudde, J. Potemra, S.-P. Xie, P. Liu, and B. Wang, 2003: Coupled dynamics in the Indian Ocean: Spring initiation of the zonal mode. *Deep-Sea Res.,* **50B,** 2305–2330.

——, P. Liu, and S. P. Xie, 2005: Southwest Indian Ocean SST variability: Its local effect and remote influence on Asian monsoons. *J. Climate,* **18,** 4150–4167.

Ashok, K., Z. Guan, and T. Yamagata, 2003: Influence of the Indian Ocean dipole on the Australian winter rainfall. *Geophys. Res. Lett.,* **30,** 1821, doi:10.1029/2003GL017926.

——, S. Behera, S. Rao, H. Weng, and T. Yamagata, 2007: El Niño Modoki and its possible teleconnection. *J. Geophys. Res.,* **112,** C11007, doi:10.1029/2006JC003798.

Cai, W., A. Sullivan, and T. Cowan, 2009: Rainfall teleconnections with Indo-Pacific variability in the WCRP CMIP3 models. *J. Climate,* **22,** 5046–5071.

Carvalho, L. M. V., C. Jones, and T. Ambrizzi, 2005: Opposite phases of the Antarctic Oscillation and relationships with intraseasonal to interannual activity in the tropics during the austral summer. *J. Climate,* **18,** 702–717.

Chambers, D. P., B. D. Tapley, and R. H. Stewart, 1999: Anomalous warming in the Indian Ocean coincident with El Niño. *J. Geophys. Res.,* **104,** 3035–3047.

Collins, W. D., P. J. Rasch, B. A. Boville, J. J. Hack, J. R. McCaa, D. L. Williamson, J. T. Kiehl, and B. Briegleb, 2004: Description of the NCAR Community Atmosphere Model (CAM 3.0). NCAR Tech. Note NCAR/TN-464+STR, 226 pp.

Chan, S., S. Behera, and T. Yamagata, 2008: Indian Ocean dipole influence on South American rainfall. *Geophys. Res. Lett.,* **35,** L14S12, doi:10.1029/2008GL034204.

Deser, C., M. A. Alexander, S.-P. Xie, and A. S. Phillips, 2010: Sea surface temperature variability: Patterns and mechanisms. *Ann. Rev. Mar. Sci.,* **2,** 115–143.

Drumond, A. R. de M., and T. Ambrizzi, 2008: The role of the south Indian and Pacific Oceans in South American monsoon variability. *Theor. Appl. Climatol.,* **94,** 125–137.

Du, Y., S.-P. Xie, G. Huang, and K. Hu, 2009: Role of air–sea interaction in the long persistence of El Niño–induced North Indian Ocean warming. *J. Climate,* **22,** 2023–2038.

Gill, A. E., 1980: Some simple solutions for heat-induced tropical circulation. *Quart. J. Roy. Meteor. Soc.,* **106,** 447–462.

Hoskins, B. J., and D. J. Karoly, 1981: The steady linear response of a spherical atmosphere to thermal and orographic forcing. *J. Atmos. Sci.,* **38,** 1179–1196.

Huang, G., K. Hu, and S.-P. Xie, 2010: Strengthening of tropical Indian Ocean teleconnection to the northwest Pacific since the mid-1970s: An atmospheric GCM study. *J. Climate,* **23,** 5294–5304.

Jones, D., W. Wang, and R. Fawcett, 2009: High-quality spatial climate data-sets for Australia. *Aust. Meteor. Oceanogr. J.,* **58,** 233–248.

Klein, S. A., B. Soden, and N. C. Lau, 1999: Remote sea surface temperature variations during ENSO: Evidence for a tropical atmospheric bridge. *J. Climate,* **12,** 917–932.

Lau, N.-C., and M. J. Nath, 2000: Impact of ENSO on the variability of the Asian–Australian monsoons as simulated in GCM experiments. *J. Climate,* **13,** 4283–4309.

——, and ——, 2003: Atmosphere–ocean variations in the Indo-Pacific sector during ENSO episodes. *J. Climate,* **16,** 3–20.

Lee, S.-K., C. Wang, and B. E. Mapes, 2009: A simple atmospheric model of the local and teleconnection responses to tropical heating anomalies. *J. Climate,* **22,** 272–284.

L'Heureux, M. L., and D. W. J. Thompson, 2006: Observed relationships between the El Niño–Southern Oscillation and the extratropical zonal-mean circulation. *J. Climate,* **19,** 276–287.

Li, S., J. Lu, G. Huang, and K. Hu, 2008: Tropical Indian Ocean basin warming and East Asian summer monsoon: A multiple AGCM study. *J. Climate,* **21,** 6080–6088.

Li, T., B. Wang, C.-P. Chang, and Y. Zhang, 2003: A theory for the Indian Ocean dipole–zonal mode. *J. Atmos. Sci.,* **60,** 2119–2135.

Luffman, J. J., A. S. Taschetto, and M. H. England, 2010: Global and regional climate response to late twentieth-century warming over the Indian Ocean. *J. Climate,* **23,** 1660–1674.

Masumoto, Y., and G. Meyers, 1998: Forced Rossby waves in the southern tropical Indian Ocean. *J. Geophys. Res.,* **103,** 27 589–27 602.

Meyers, G., P. McIntosh, L. Pigot, and M. Pook, 2007: The years of El Niño, La Niña, and interactions with the tropical Indian Ocean. *J. Climate,* **20,** 2872–2880.

Rayner, N. A., D. E. Parker, E. B. Horton, C. K. Folland, L. V. Alexander, D. P. Rowell, E. C. Kent, and A. Kaplan, 2003: Global analyses of sea surface temperature, sea ice, and night marine air temperature since the late nineteenth century. *J. Geophys. Res.,* **108,** 4407, doi:10.1029/2002JD002670.

Reynolds, R. W., N. A. Rayner, T. M. Smith, D. C. Stokes, and W. Wang, 2002: An improved in situ and satellite SST analysis for climate. *J. Climate,* **15,** 1609–1625.

Risbey, J. S., M. J. Pook, P. C. McIntosh, M. C. Wheeler, and H. H. Hendon, 2009: On the remote drivers of rainfall variability in Australia. *Mon. Wea. Rev.,* **137,** 3233–3253.

Saji, N. H., and T. Yamagata, 2003: Structure of SST and surface wind variability during Indian Ocean dipole mode events: COADS observations. *J. Climate,* **16,** 2735–2751.

——, B. N. Goswami, P. N. Vinayachandran, and T. Yamagata, 1999: A dipole mode in the tropical Indian Ocean. *Nature,* **401,** 360–363.

——, T. Ambrizzi, and S. E. T. Ferraz, 2005: Indian Ocean dipole mode events and austral surface temperature anomalies. *Dyn. Atmos. Oceans,* **39,** 87–102.

Schott, F. A., S.-P. Xie, and J. P. McCreary Jr., 2009: Indian Ocean circulation and climate variability. *Rev. Geophys.,* **47,** RG1002, doi:10.1029/2007RG000245.

Suppiah, R., 1992: The Australian summer monsoon: A review. *Prog. Phys. Geogr.,* **16,** 283–318.

Taschetto, A. S., and M. H. England, 2009: El Niño Modoki impacts on Australian rainfall. *J. Climate,* **22,** 3167–3174.

——, C. C. Ummenhofer, A. Sen Gupta, and M. H. England, 2009: Effect of anomalous warming in the central Pacific on the Australian monsoon. *Geophys. Res. Lett.,* **36,** L12704, doi:10.1029/2009GL038416.

——, R. J. Haarsma, A. Sen Gupta, C. C. Ummenhofer, K. J. Hill, and M. H. England, 2010: Australian monsoon variability driven by a Gill–Matsuno-type response to central west Pacific warming. *J. Climate,* **23,** 4717–4736.

Tokinaga, H., and Y. Tanimoto, 2004: Seasonal transition of SST anomalies in the tropical Indian Ocean during El Niño and Indian Ocean dipole years. *J. Meteor. Soc. Japan,* **82,** 1007–1018.

Ummenhofer, C. C., M. H. England, P. C. McIntosh, G. A. Meyers, M. J. Pook, J. S. Risbey, A. S. Gupta, and A. S. Taschetto, 2009a: What causes southeast Australia's worst droughts? *Geophys. Res. Lett.,* **36,** L04706, doi:10.1029/2008GL036801.

——, A. Sen Gupta, A. S. Taschetto, and M. H. England, 2009b: Modulation of Australian precipitation by meridional gradients in east Indian Ocean sea surface temperature. *J. Climate,* **22,** 5597–5610.

Wang, B., I.-S. Kang, and J.-Y. Lee, 2004: Ensemble simulations of Asian–Australian monsoon variability by 11 AGCMs. *J. Climate,* **17,** 803–818.

——, J.-Y. Lee, I.-S. Kang, J. Shukla, J.-S. Kug, A. Kumar, J. Schemm, J.-J. Luo, T. Yamagata, and C.-K. Park, 2008: How accurately do coupled climate models predict the leading modes of Asian–Australian monsoon interannual variability? *Climate Dyn.,* **30,** 605–619.

Wang, G., and H. H. Hendon, 2007: Sensitivity of Australian rainfall to inter–El Niño variations. *J. Climate,* **20,** 4211–4226.

Watanabe, M., and F.-F. Jin, 2002: Role of Indian Ocean warming in the development of Philippine Sea anticyclone during ENSO. *Geophys. Res. Lett.,* **29,** 1478, doi:10.1029/2001GL014318.

Xie, S. P., H. Annamalai, F. A. Schott, and J. P. McCreary, 2002: Structure and mechanisms of south Indian Ocean climate variability. *J. Climate,* **15,** 864–878.

——, K. Hu, J. Hafner, H. Tokinaga, Y. Du, G. Huang, and T. Sampe, 2009: Indian Ocean capacitor effect on Indo–Western Pacific climate during the summer following El Niño. *J. Climate,* **22,** 730–747.

Yang, J., Q. Liu, S.-P. Xie, Z. Liu, and L. Wu, 2007: Impact of the Indian Ocean SST basin mode on the Asian summer monsoon. *Geophys. Res. Lett.,* **34,** L02708, doi:10.1029/2006GL028571.

——, ——, Z. Liu, L. Wu, and F. Huang, 2009: Basin mode of Indian Ocean sea surface temperature and Northern Hemisphere circumglobal teleconnection. *Geophys. Res. Lett.,* **36,** L19705, doi:10.1029/2009GL039559.

Zhou, T., B. Wu, and B. Wang, 2009: How well do atmospheric general circulation models capture the leading modes of the interannual variability of the Asian–Australian monsoon? *J. Climate,* **22,** 1159–1173.